Determination of the Optimal Crystal Cut and Propagation Direction of a Piezoelectric Substrate for SAW Devices

탄성표면파 소자용 압전기판의 최적 절단면과 전파방향 결정

Yongrae Roh*, Young Ho Bae*, Dae-Sik Chung*
노 용 래*, 배 영 호*, 정 대 식*

ABSTRACT

Characteristics of a piezoelectric material are evaluated to pick up the optimal crystal cut and propagation direction for a SAW device. For the piezoelectric single crystal $LiTaO_3$, such items are investigated as the Rayleigh wave velocity, the electromechanical coupling factor, the surface permittivity, the frequency-temperature coefficient, the air loading attenuation, the pure mode propagation, the beam steering and the misalignment sensitivity. Theoretical calculations reveal that Y-cut and Z propagation is the optimal SAW propagation path. The results are confirmed through experiments. The method employed in this paper is applicable to other crystals, too, either single or poly crystals.

요 약

탄성표면파 소자용 압전재료의 특성을 검사하여 최적 절단면과 전파방향을 결정하였다. 압전단결정 $LiTaO_3$에 대하여 Rayleigh파의 속도, 전기기계결합계수, 표면유전상수, 주파수 온도계수, 감쇠계수, 파이프모드 전파, 빔 조향, 그리고 정렬오차 감도 등의 항목들을 평가하였다. 이론적 계산 결과 Y절단Z전파의 X축 방향이 최적적로 나타났고, 이 결과는 실험에 의해 확인되었다. 본 논문의 평가방법은 여타 다른 압전재료들에도 동일하게 적용이 가능하다.

I. Introduction

Surface acoustic wave device technology has now advanced to the point where a large number of different components are being manufactured. These components can be generally classified as passive devices on piezoelectric substrates. Piezoelectricity is the phenomenon that couples elastic stresses and strains to electric fields and displacements. It occurs only in anisotropic materials whose internal structure lacks a center of symmetry. That is their SAW propagation characteristics are not constant in all directions. For a surface wave device, the choice of an appropriate material for a substrate is a vital part of the design procedure. There are a number of materials available to the SAW component designer: the choice depends on the type of the device to be prepared, the frequency of operation, the bandwidth, the time delay, and the system use. The

*RIST
접수일자 : 1993년 10월 18일

...important parameters for a material are the ... coupling and the temperature coef... Large values of the coupling generally ... lower insertion losses for devices, though ... also give stronger electrode interactions and ... are not always desirable. The tradeoffs might ... the obvious one of high electromechanical coupling versus low temperature coefficient of delay, or might involve other factors such as availability of sufficiently large substrates, compatibility with fabrication techniques, spurious signal reflection, acoustic loss, or cost.

In this paper, characteristics of a piezoelectric material are evaluated for its various crystal cuts and directions to pick up the optimum orientation for the use as a substrate of a SAW device. Our specific application of the device is SAW chemical sensors. The single crystal $LiTaO_3$ is chosen for the substrate material due to its high coupling factor, low temperature coefficient, and easy availability. Of the many criteria to evaluate the performance of a piezoelectric substrate, eight main items are selected such as the velocity, the coupling factor, the surface permittivity, the frequency temperature coefficient, the air loading attenuation, the pure mode propagation, the beam steering and the misalignment sensitivity [2]. These eight items are estimated for each combination of the $LiTaO_3$ cut and the SAW propagation direction. Our requirements for a SAW sensor are that the device should have a high coupling factor, a low temperature coefficient and so on. Analysis of the results with these conditions in mind reveals the optimum orientation. Nearly always, the material and orientation are chosen such that only one surface wave mode can be excited. We prefer the orientation such that the one surface wave mode is a piezoelectric Rayleigh wave. Bleustein-Gulyaev waves are excluded because their large penetration depths would require thicker substrates in order to avoid coupling to the rear surface [3]. Section 2 describes the calculation and selection procedures for each of the criteria. The combinations of crystal cuts and SAW propagation directions are very large. The selection strategy is applied to several representative orientations of the crystal with the help of crystal symmetries. In Sec. 3, validity of the selection is confirmed through real fabrication and performance measurement of SAW devices. For our sensing purpose, fabrication of fantastic IDTs is not of great interest. We employ a rather simple single electrode IDT. Discussion of the results is conducted in the final section.

II. Numerical Calculation

The piezoelectric single crystal $LiTaO_3$ is chosen for the substrate material of a SAW device. Material properties of the crystal are cited from Ref. 4. We apply the eight criteria in Sec. 1 to a variety of cuts and axes of the wafer to pick up the optimum orientation. Figure 1 is the Cartesian coordinate employed in the numerical analysis of the SAW propagation. The crystal axes X, Y and Z are transformed to the geometrical coordinate axes x, y and z with appropriate Euler angles. Transformation rule is the well-known orthogonal coordinate rotation law [5]. Simulation algorithm for general Rayleigh wave propagation is described in Ref. 6 and is not repeated here.

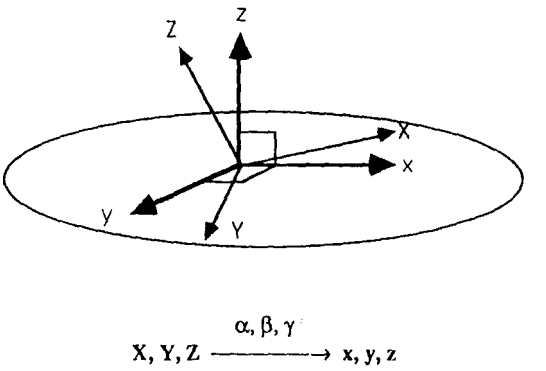

Figure 1. Coordinate transformation from crystal axes X, Y and Z to geometrical axes x, y and z. α, β and γ are Euler angles describing each rotation.

Each criterion and corresponding calculation method is described as follows. Results are displayed for a representative case, i.e., Y-cut plane.

2.1. SAW Velocity

The first design consideration is SAW velocity. In order to achieve a very long delay time, the orientation with relatively high velocity will be desirable to minimize the device size. On the other hand, high velocity implies closely spaced [illegible] transducer fingers and may lead to fabrication difficulty and low yield [7]. There should be some tradeoff. However, unless the velocity difference for different orientations is very large, the absolute velocity should not be a major condition to choose a material. Figure 2-a shows variation of the velocity with propagation directions on the Y cut plane. Denoted values are unstiffened velocity (v_0), that is the velocity before the application of excitation voltage to the substrate surface. Similar results displayed in Fig. 2 b when an electric field is put on the surface. It is stiffened velocity v_s. The two values are utilized to calculate piezoelectric coupling factors at the next section. For our purpose, the direction of high velocity is desirable, which leads to the selection of the Z axis on the plane.

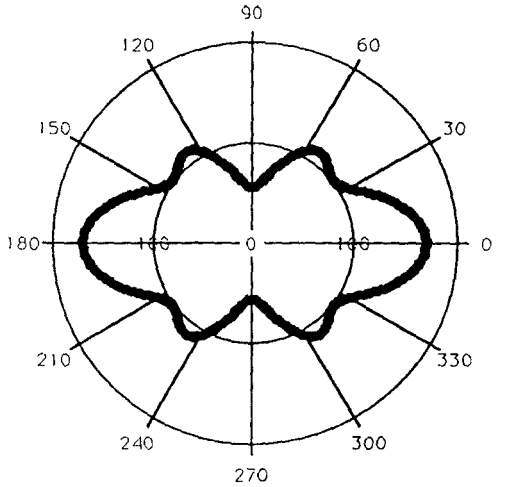

(a) Unstiffened velocity

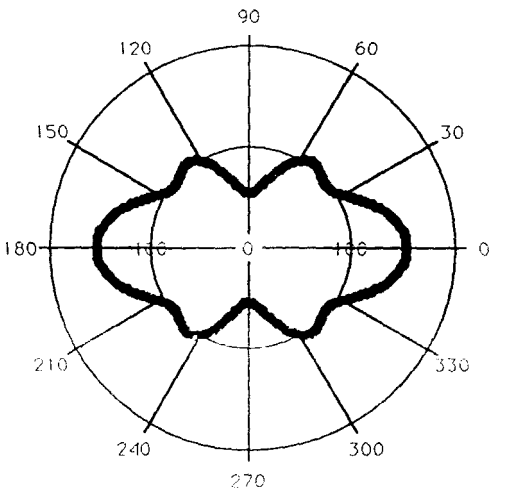

(b) Stiffened velocity

Figure 2. Variation of Rayleigh wave velocity on the Y-cut plane. Angle θ is the crystal Z-axis and numbers on the circumference means that much rotation in degrees from the Z-axis. Numbers on the radius added with 3100 are absolute velocity of the wave.

2.2. Electromechanical Coupling Factor

The electromechanical coupling constant k^2 for surface acoustic waves can not be readily calculated from the piezoelectric and elastic constants. However, it can be related to the fractional change in SAW velocity when a thin, massless conductor is deposited on the propagation surface [8] as noted in

$$k^2 = 2(1+\varepsilon_0/\varepsilon_p^1)\,\Delta v/v_s(1-\Delta v/v_s) \tag{1}$$

where Δv is $v_0 - v_s$, ε_0 is the dielectric constant of free space and

$$\varepsilon_p^1 = (\varepsilon_{11}^1\varepsilon_{33}^1 - \varepsilon_{13}^{1\,2})^{1/2}. \tag{2}$$

ε_p^1 is named the surface permittivity of the substrate. The ε_{ij}^1 are the dielectric constants of the piezoelectric substrate with the coordinate in Fig. 1. The superscript T means measurement at constant stress. Figure 3 shows the results evaluated on the Y-cut plane. Strong piezoelectric coupling is desirable for our purpose and, hence, the Z axis is the best.

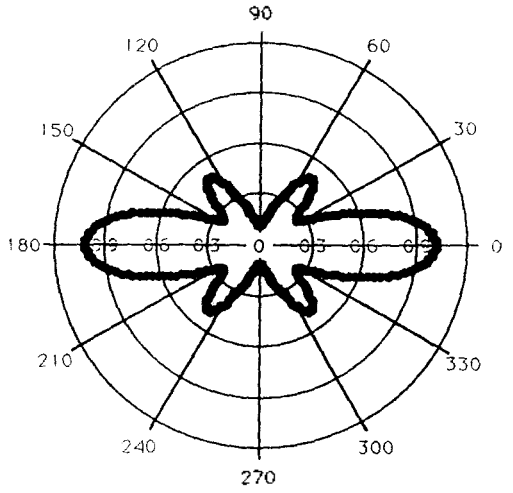

Figure 3. Variation of the coupling factor on the Y-cut plane. Angle 0 is the crystal Z-axis and numbers on the circumference means that much rotation in degrees from the Z-axis. Numbers on the radius are absolute values of the factor in percent.

2.3. Surface Permittivity

The surface permittivity ε_p^s works as a part of the effective permittivity($=\varepsilon_0+\varepsilon_p^s$) as investigated by Ingebrigtsen [9]. The effective permittivity relates the surface potential ϕ and charge density σ generated by IDTs, and its relationship is determined with appropriate boundary conditions. Following Ingebrigtsen, in the quasi-static approximation, the potential ϕ of the surface wave radiation in the x direction is

$$\phi(x,\omega) = i\Gamma\,\sigma(k_0,\omega)\exp(ik_0 x) \tag{3}$$

and power P carried by this wave is

$$P = \frac{1}{4}\,\omega\, W|\phi(\omega)|^2/\Gamma \tag{4}$$

where k_0 is the wave number, ω is the frequency, W is the width of an IDT, and Γ is $\dfrac{1}{\varepsilon_0+\varepsilon_p^s}\dfrac{v_0-v_s}{v_0}$. Large ϕ and P requires large Γ that corresponds to small ε_p^s. ε_p^s is also involved in the coupling factor k^2 as in Eq. 1. For large k^2, small ε_p^s is desirable, again. However, ε_p^s is usually almost constant for various cuts and directions of a given crystal. Hence it must be a secondary factor to be considered. Figure 4 shows the calculation results on the plane of Y-cut.

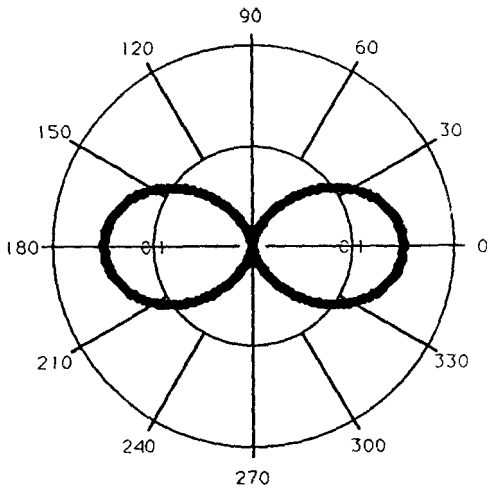

Figure 4. Variation of the surface permittivity on the Y-cut plane. Angle 0 is the crystal Z-axis and numbers on the circumference means that much rotation in degrees from the Z-axis. Numbers on the radius added with 42.6 are absolute values of $\varepsilon_p^s/\varepsilon_0$.

2.4. Frequency-Temperature Coefficient(FTC)

One of the most annoying sources of noise and instability of a SAW device is its sensitivity to environmental temperature variation [10]. It is desirable for a particular cut and crystal axis to have an almost negligible temperature coefficient concerning SAW propagation. For each point to be tabulated, we fix a reference temperature (25℃) and calculate the phase velocity at another temperature $T+\Delta T$ where ΔT is set 25℃. The velocity at 25℃ has been already determined in Sec. 2.1. With the two phase velocities, FTC is obtained as follows.

$$FTC \approx \frac{\Delta V}{\Delta T\, V_{01}} * 10^6\ (\text{ppm}) \tag{5}$$

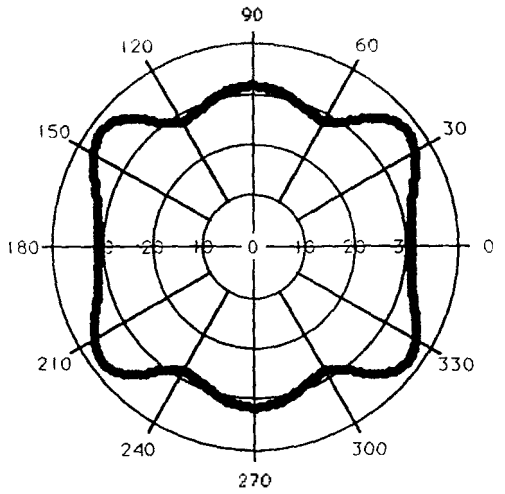

Figure 5. Variation of the FTC on the Y-cut plane. Angle θ is the crystal Z axis and numbers on the circumference means that much rotation in degrees from the Z-axis. Numbers on the radius are absolute values of the FTC in ppm.

where ΔV is $V_{01} - V_{02}$, V_{01} is the unstiffened Rayleigh wave velocity at 25℃ and V_{02} is that at 50 ℃. Variation of the FTC on the Y-cut plane is described by Fig. 5. Z axis and 60℃ rotated Z axis are preferred for our purpose.

2.5. Air Loading Attenuation

Acoustic surface wave propagation along the boundary between a solid and a low density fluid results in both attenuation along the direction of of propagation and perturbation of the vacuum Rayleigh wave velocity [11]. At microwave frequencies, the attenuation of this leaky wave due to propagation in air can result in significant increase in device insertion loss. Much of experimental and theoretical work has been done to estimate this air loading effect. In this paper, the approximate theory developed by Artz and coworkers are cited due to its excellent coherence with measurements [12]. According to Artz, the attenuation coefficient α due to gas loading can be expressed in the following form.

$$\alpha = \rho_g V_g / \rho_s V_s \lambda_s \text{ (Nepers/m)} \quad (6)$$

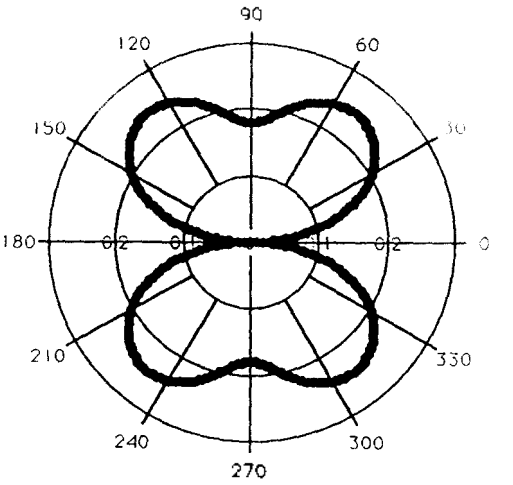

(a) C_0

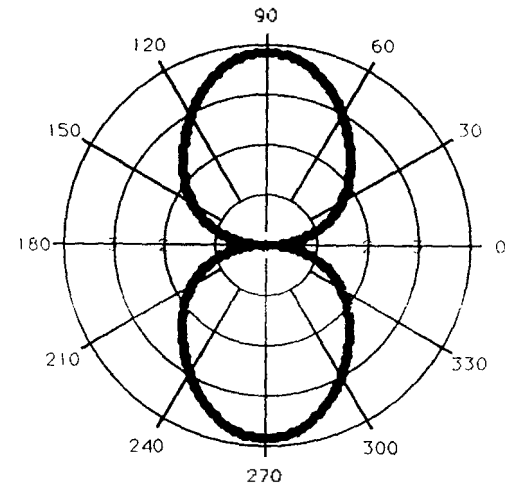

(b) e_0

Figure 6. Variation of the C_0 and e_0 on the Y-cut plane. Angle θ is the Z-axis and numbers on the circumference means that much rotation in degrees from the Z-axis. Numbers on the radius are magnitudes of the C_0 and e_0, whose absolute value has no meaning.

where ρ_g is the density of the gas, V_g is the longitudinal wave velocity in the gas, ρ_2 is the density of the surface wave substrate, V_s is the Rayleigh wave velocity, and λ_s is the Rayleigh wave wavelength. Center frequency of the SAW is assumed to be 1 MHz. Figure 7 shows calculation results

of the Y cut plane with an loading where ρ_s is 1, ε_0 is 8.854×10^{-12} and V_s is 3140 m/s.

2.6. Pure Mode Propagation

When an electric field is applied to an anisotropic piezoelectric substrate by means of an IDT, several different types of SAWs can be generated simultaneously depending on the geometry of a device. For energy efficiency and low noise, only the mode of interest should be generated, which is possible only in the pure mode propagation [3]. In pure mode directions, the Rayleigh wave is not coupled with other types of SAWs like Love waves. Generated Rayleigh wave has displacements in longitudinal and shear vertical directions only. Some workers confuse pure mode propagation with no beam steering propagation. We differentiate one from the other in that the direction of no beam steering does not guarantee no coupling of the Rayleigh wave with other types of SAWs. To be pure mode, the material constants connecting the fields in shear horizontal direction with those in the sagittal plane(a vertical plane normal to the wavefront) should be zero for that particular crystal cut and axis. In the secular equation of the SAW [6], we should have null values for the elastic stiffness constants C_{11}, C_{16}, C_{31}, C_{36}, C_{51} and C_{56} as well as the piezoelectric constants e_{11}, e_{16}, e_{31} and e_{36}. Here the material constants are the values transformed with appropriate Euler angles describing each orientation. Figure 6-a shows the variation of the value

$$C_{11} = C_{14}^2 + C_{16}^2 + C_{34}^2 + C_{36}^2 + C_{54}^2 + C_{56}^2 \quad (7)$$

while Fig. 6-b does that of the value

$$e_{11} = e_{14}^2 + e_{16}^2 + e_{34}^2 + e_{36}^2. \quad (8)$$

The figures reveal that Z axis is the only pure mode direction.

2.7. Beam Steering

Usually the distance between input and output

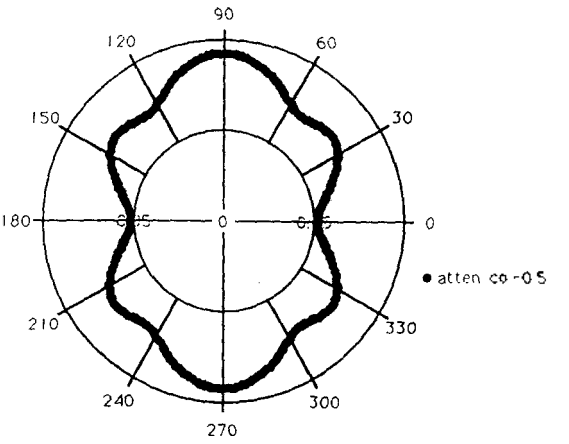

Figure 7. Variation of the attenuation coefficient α on the Y cut plane. Angle 0 is the crystal Z axis and numbers on the circumference means that much rotation in degrees from the Z axis. Numbers on the radius are absolute values of the α in Nepers.

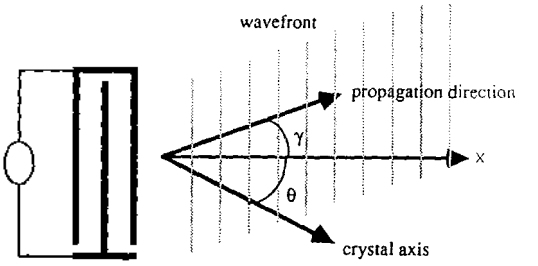

(a) Schematic diagram of beam steering. γ is the beam steering angle and θ is the orientation of the nominal SAW propagation direction from the crystal axis

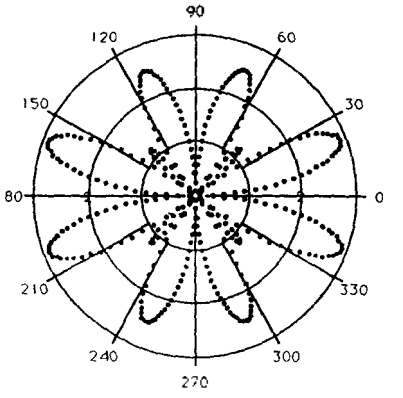

(b) Variation of the beam steering angle γ

Figure 8. Variation of the beam steering angle γ on the Y-cut plane. Angle 0 is the crystal Z axis and numbers on the circumference means that much rotation in degrees from the Z axis. Numbers on the radius are absolute values of the γ in degrees.

IDTs are set within the near field range of the electrodes. In the near field, the waves due to an aperture with uniform illumination exhibit little diffraction spreading, so that diffraction need not be taken into account. However, apart from the diffraction, anisotropic materials can exhibit beam steering, which causes the beam to propagate in a direction not normal to the wavefronts [13]. Avoidance of beam steering requires very accurate orientation of the crstalline substrate surface relative to the crystal axes as well as accurate alignment of the IDT.

As shown in Fig. 8-a, in the near field, the disturbance propagates with no distortion, but the propagation direction of the beam makes an angle γ with the x axis, that is, with the direction normal to the wavefronts. The angle γ is called the beam steering angle, and generally depends on the orientation angle. From Ref. 13, wh have

$$\text{Tan}\,\gamma = \frac{1}{v_n}\frac{dv_n}{d\theta} \tag{9}$$

The smaller is the γ, the better is the device performance. A more rigorous derivation is obtained by defining a Poynting vector for an elastic piezoelectric medium, analogous to the electromagnetic wave propagation [14]. Figure 8-b displays variation of the γ on the Y-cut plane, Z axis and every 45° rotated direction form the Z axis are desirable

2.8. Misalignment Sensitivity

In the case γ is zero, however, beam steering can still arise in practice because of an error in the angle θ due to misalignment of an IDT [1]. The degree of the misalignment effect depends

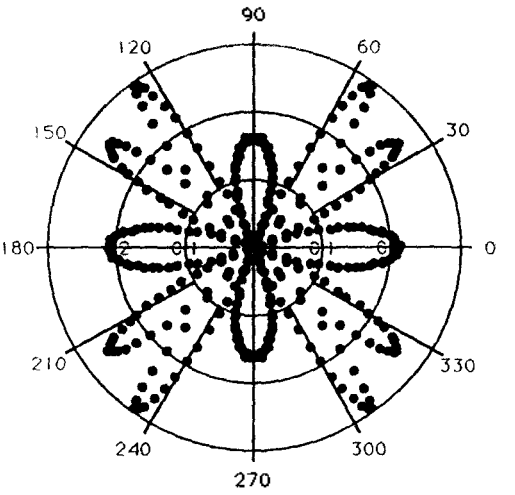

Figure 9. Variation of the misalignment sensitivity on the Y-cut plane. Angle 0 is the crystal Z-axis and numbers on the circumference means that much rotation in degrees from the Z-axis. Numbers on the radius are absolute values of the sensitivity.

on anisotropy characteristics of the substrate material. For small errors, γ can be found from the equation given by

$$\frac{d\gamma}{d\theta} = \frac{1}{v_n}\frac{d^2v_n}{d\theta^2}\,\text{Cos}^2\gamma - \text{Sin}^2\gamma. \tag{10}$$

The value $\frac{d\gamma}{d\theta}$ is defined misalignment sensitivity. In principle, the misalignment error should be a secondary factor because every possible method is usually taken to preserve precise alignment even though it may cause severe errors in practical fabrication. Figure 9 shows the sensitivity variation on the Y-cut plane.

So far, we have illuminated individual criterion to judge the suitability of a certain orientation of the substrate for a SAW device. For selection of the optimal orientation, the whole effects of the above eight criteria should be analyzed with a certain scheme of priority. Once the scheme is set up, the calculation is performed for various cuts and directions of the $LiTaO_3$ substrate. The number of combinations of crystal cuts and propagation directions is very large. It is somewhat

Table 1. Calculation results of the eight items for representative symmetric orientations of $LiTaO_3$

cut	prop. direction	C_0+e_0	k2 (%)	FTC (ppm)	α	γ	V_0	$\varepsilon_0^1/\varepsilon_0$	misalign. sen.
	priority	*1*	*2*	*3*	*4*	*5*	*6*	*7*	*8*
Z cut	X axis	1.817	0.107	50.00	0.566	0.0	3229	42.75	0.406
	30 rotated X axis	0.000	0.796	52.47	0.529	0.0	3340	42.71	1.090
	60 rotated X axis	1.817	0.107	50.00	0.566	0.0	3229	42.64	0.406
	90 rotated X axis	0.000	0.796	52.47	0.529	0.0	3341	42.60	1.090
167 Z cut	Y axis	0.000	0.337	56.31	0.562	0.0	3241	42.75	0.501
	67 rotated Y axis	1.011	1.047	49.05	0.517	0.0	3378	42.74	1.101
	90 rotated Y axis	0.522	0.293	51.45	0.546	0.0	3287	42.74	0.558
Y cut	Z axis	0.000	1.021	30.81	0.552	0.0	3270	43.75	0.210
	38 rotated Z axis	3.080	0.448	28.55	0.573	0.0	3208	43.64	0.245
	90 rotated Z axis	4.026	0.119	31.60	0.593	0.0	3155	42.60	0.162
36 Y cut	X axis	2.387	0.293	32.92	0.544	0.0	3294	42.65	0.371
	27 rotated X axis	0.000	1.070	26.22	0.537	0.0	3315	43.67	0.357
	90 rotated X axis	2.977	0.408	40.12	0.573	0.0	3208	42.75	0.330
X cut	138 rotated Y axis	3.335	0.011	41.92	0.602	0.0	3132	42.67	0.121

wasting time and computer operation cost to construct whole stereographic projects through complete calculation. However, with the help of crystal symmetry, we can conjecture the total three dimensional behavior of the material through analysis of several representative cases. $LiTaO_3$ has trigonal 3m symmetry, which means that it has one three-fold axis and three mirror planes [15]. Hence the information on any one side of the symmetric axes and mirror planes is sufficient to derive the whole idea. Table 1 illustrates the results for the cases of primary crystal symmetry. All the values on the table have corresponding physical implications except the C_0+e_0 that is scaled down arbitrarily for convenience. The above technique can be employed for arbitrary SAW device applications. However, different applications require different conditions to be met. The main motivation of current study is to develop a SAW chemical sensor. Our use of a SAW sensor requires such primary factors as (1) pure mode propagation (i.e., $C_0=e_0=0$), (2) the maximum coupling factor, (3) the minimum FTC, (4) the minimum air loading attenuation, and (5) no beam steering angle. Secondary considerations include (1) the maximum velocity, (2) the minimum surface permittivity, and (3) the minimum misalignment sensitivity. In this sense, the orientations of Y-cut, Z-axis and 36° rotated Y-cut,

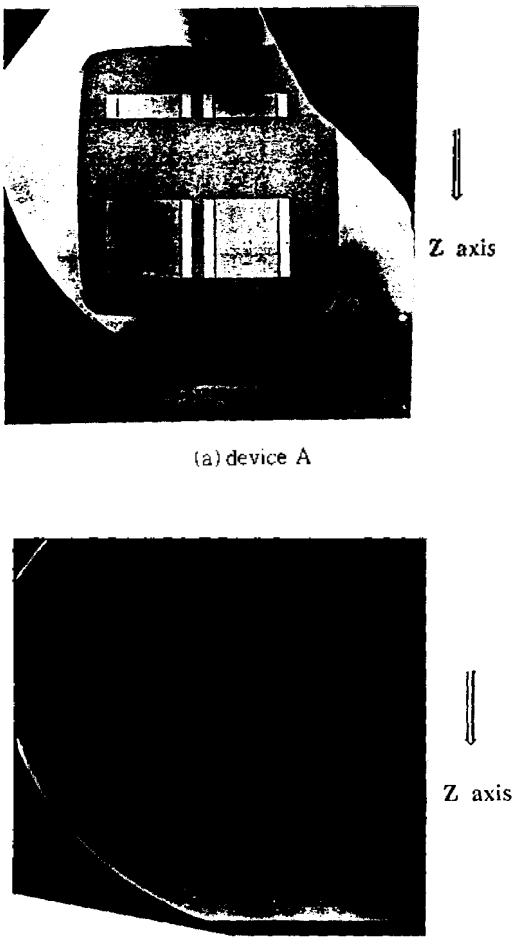

(a) device A

(b) device B

Figure 10. Photographs of the SAW devices A and B.

27° rotated X-axis are the best candidates. Both of them show quite similar performance. However, it is very difficult to achieve the direction of 36° rotated Y-cut and 27° rotated X-axis in real processing of the wafer. Difficulty in processing can impose inherent errors in alignment of IDTs. Therefore, the optimum orientation is determined to be the Y-cut and Z-axis.

Ⅲ. Experiments

To check validity of the results in the previous section, we manufactured SAW devices for two selective crystal cuts. The first device (A) has the crystal cut and propagation direction oriented at Y-cut and Z-axis. The second device (B) has the orientation of Y-cut and 45° rotated Z-axis. Test samples are from Yamazu [16]. Figure 10 shows the devices. The devices are designed to be a dual type in order to allow reliable noise reduction in the future operation of the sensor. The IDTs on all the devices are standard single electrode type. Input IDTs have sixty-four electrode pairs and output IDTs have twenty pairs. Center frequency is set to be approximately 40 MHz for the Y-cut and Z-axis propagation. Performance of the devices is investigated with a HP network analyzer 8752A. The devices are not electrically or acoustically tuned for matching with the analyzer. Raw performance is checked just to see any difference between the two.

Figure 11 shows measured frequency responses of the devices. The device A has superior responses to those of the device B in view of the bandwidth, the magnitude of ripples, and the insertion loss. Especially, the bandwidth has such a difference of 26%, which can be anticipated from the results of Fig. 3. A higher coupling factor turns out a larger bandwidth as shown in the following equation [2].

$$\text{FractionalBandwidth} \propto \sqrt{\frac{4k^2}{\pi}} \tag{11}$$

The prohibitively larges insertion loss is owing to

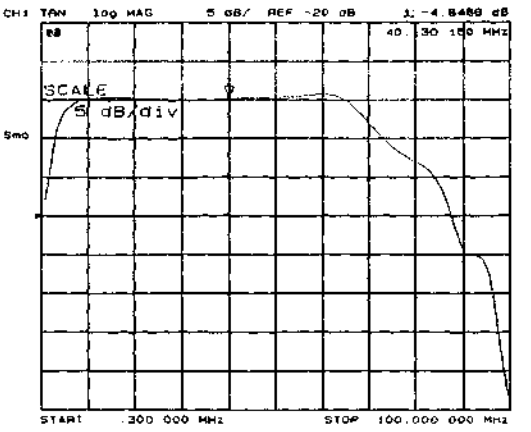

(a) device A

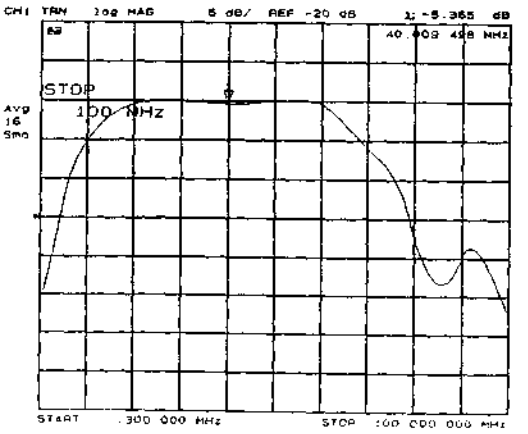

(b) device B

Figure 11. Frequency responses of the SAW devices

the mismatch of the devices with the measurement instrument. We have performed experiments just to confirm the validity of the calculation and the result is good enough not to try any more other directions.

Ⅳ. Conclusion

Characteristics of the piezoelectric single crystal $LiTaO_3$ are evaluated to determine the optimal surface orientation for use as a SAW device substrate. Investigated items are the Rayleigh wave velocity, the electromechanical coupling factor,

the surface permittivity, the air loading attenuation, the pure mode propagation, the beam steering and the misalignment sensitivity. Theoretical calculations reveal that Y-cut and Z-axis is the optimal SAW propagation path. The results are confirmed through experiments. The method employed in this paper is applicable to other crystals, too, either single or poly crystals. Similar study is underway for $LiNbO_3$ for comparison with $LiTaO_3$.

References

1. D. P. Morgan, Surface wave devices for signal processing, Elsevier, New York, 1985
2. C. Campbell, SAW devices and their signal processing applications, Academic Press, New York, 1989
3. B. A. Auld, Acoustic fields and waves in solids, vol. 2, John Wiley & Sons, New York, 1973
4. K. H. H. O. Modelung, Numerical data and functional relationships in science and technology, vol. 18: elastic, piezoelectric, pyroelectric, piezooptic, electrooptic constants and nonlinear dielectric susceptibilities of crystals, Springer-Verlag, New York, 1981
5. G. Arfken, Mathematical methods for physicists, Academic Press, New York, 1970
6. V. V. Varadan, Y. R. Roh and V. J. Varadan Proceedings of Ultrasonics Symposium, pp. 591-591 1989
7. I. D. Avramov, IEEE Transactions on Ultrasonics Ferroelectrics, and Frequency Control, vol. 38, pp 331-336, Jul. 1991
8. M. B. Schulz and J. H. Matsinger, Applied Physics Letters, vol. 22, pp. 367-369
9. K. A. Ingebrigtsen, Journal of Applied Physics, vol 40, pp. 2681-2686, 1969
10. M. Feldmann and J. Henaff, Surface acoustic waves for signal processing, Artech House, Boston, 1989
11. J. J. Campbell and W. R. Jones, IEEE Transactions on Sonics and Ultrasonics, Vol. 17, pp. 71-76, Apr. 1970
12. R. M. Artz, E. Salzmann, K. Dransfeld, Applied Physics Letter, vol. 10, p. 165, 1967
13. T. L. Szabo and A. J. Slobodnik, Jr., IEEE Transactions on Sonics and Ultrasonics, Vol. 20, pp. 240-251, Jul. 1973
14. C. T. A. Johnk, Engineering electromagnetic fields and waves, John-Wiley & Sons, New York, 1988
15. J. F. Nye, Physical properties of crystals, Oxford University Press, Oxford, 1985
16. Catalogue of Yamazu Ceramics Co. Ltd, Japan, 1992

▲Yongrae Roh

Yongrae Roh received the B. S. and M. S. degrees in Mineral and Petroleum Engineering from Seoul National University in 1984 and 1986, respectively. He got the Ph. D. degree in Engineering Science and Mechanics (major in Acoustics) from the Pennsylvania State University, U.S.A., in 1990. He is currently a senior research scientist in RIST, Pohang. Major research area includes SAW devices, ultrasonic transducers, and noise & vibration control.